Radiol Oncol 2001; 35(1): 63-71.

Design considerations for direct and indirect active matrix flat-panel portal imagers

Martin Lachaine and Biagio Gino Fallone

Department of Medical Physics, Cross Cancer Institute, University of Alberta, Alberta, Canada
Department of Physics, McGill University, Montreal, Canada

Background. *Recent advances in thin film transistor (TFT) technology have allowed the construction of active matrix flat-panel imagers (AMFPI) for various medical imaging modalities. Since the design of such systems is still in the development stage, it is unclear what detector characteristics are required in order to optimize these detectors for portal imaging.*
Material and methods. *In this work, we used cascade analysis and Monte Carlo techniques to calculate the DQE for both direct and indirect AMFPIs for portal imaging, and use these calculations to study the optimal detector characteristics. We validate our calculations with existing experimental data.*
Results. *We show that the for ideal flat-panel characteristics the direct and indirect detection methods have the same DQE for a given mass thickness.*
Conclusions. *We generate graphs which may be helpful in the design of future megavoltage AMFPIs.*

Key words: portal imaging, Monte Carlo method; DQE, AMFPI, EPID; amorphous selenium

Introduction

During a radiation therapy treatment, many factors may influence the proper delivery of a calculated dose distribution. Some of these factors include misalignment of the treatment beam with respect to the patient, external or internal patient motion, or inaccurate positioning of beam-modifying devices.[1] In order to quantify these geometric inaccuracies during treatment, a portal image is typically extracted from the megavoltage treatment beam with a radiation-sensitive detector. In this manner it is possible to verify the position of the radiation field relative to the bony anatomy. Portal imaging has also been studied with varying success for use in exit dosimetry, where the images are used to verify the dose distributions delivered to the patient.[2,3]

Traditionally, film has been used as the portal imaging detector. Over the past decade, several electronic portal imaging devices (EPIDs) have been developed for the

Received 20 October 2000
Accepted 20 November 2000

Correspondence to: Prof. B. Gino Fallone, PhD, FCCPM, ABMP, Medical Physics, Cross Cancer Institute and University of Alberta, 11560 University Avenue, Edmonton, Alberta T6G 1Z2, Canada. Phone: +1 780 432-8750; Fax: +1 780 432-8615; E-mail: Gino.fallone@cancerboard.ab.ca

purpose of replacing film.[4] The inherent advantages of such inherently digital detectors include immediate viewing and the ability to use contrast-enhancing algorithms to improve image quality. Despite these advantages, however, EPIDs have not widely replaced portal films. This has been attributed to poor image quality, limited field of view, and bulkiness.[5]

In recent years, thin film transistor (TFT) technology has lead to the development of a new category of digital x-ray detectors.[6-8] Such detectors, often called *active-matrix flat panel imagers* (AMFPIs), may use either the *indirect* or the *direct* detection of x-rays to form the digital image. The indirect method typically uses a phosphor to convert the incident x-rays into visible light, which are then converted into electron-hole pairs by an array of photodiodes. The charge is collected in the photodiodes during the image formation, and subsequently read out electronically. The direct method, on the other hand, uses a photoconductor such as amorphous selenium (*a*-Se) to directly convert the x-rays into electron-hole pairs, which are collected at pixel electrodes through the use of an applied electric field. The charges are stored in the capacitors of the active matrix during irradiation and subsequently read out.

Characteristics which must be considered when designing AMFPI detectors include the detection method (indirect or direct), detector thickness, pixel size, fill factor, and electronic noise characteristics. Some of these are difficult to quantify experimentally, since construction of AMFPIs is expensive. For this reason, it is useful to use theoretical techniques to describe AMFPI image quality, which is often quantified in terms of the detective quantum efficiency (DQE).

Cascaded systems analysis[9] has successfully been applied to calculate the DQE of AMFPI detectors in the diagnostic energy range.[10,11] These analyses have been useful in studying detector designs for various modalities such as mammography, chest radiography and fluoroscopy. At the energies used in these modalities, there is little spread of the ionizing radiation within the detector and thus this spreading is not taken into account in the analysis. At megavoltage energies, however, x-rays produce high energy electrons within a metal build-up layer (conversion plate) which is placed above the sensitive volume of the detector. These high energy electrons scatter within the detector, resulting in an additional loss of resolution.

Bissonnette *et al.*[12,13] have taken this additional process into account to model both video-based and indirect AMFPI portal imagers. Their analysis, however, did not agree with data measured by Munro and Bouius.[14] This disagreement was attributed to the fact that it is impossible to experimentally separate the spread of high-energy radiation from the spread of the visible light within the phosphor. In our work, we use Monte Carlo methods to investigate this particular problem for both direct and indirect portal AMFPIs.

The design constraints for portal AMFPIs are different than for diagnostic AMFPIs, and have to date not been studied. We thus use the cascade analysis formalism to explore potential benefits of the direct versus the indirect detection methods for portal imaging, and to explore the effects of detector thickness, pixel size, fill factor and electronic noise on the DQE at megavoltage energies for both indirect and direct detection techniques.

Materials and methods

We first consider the interaction of quanta with the detector, which are referred to as *analog* processes. We make the approximation that these can be divided into elementary *amplification* stages (which includes binary selection as a special case) and *dislocation* stages according to cascade analysis.[9,15] We neglect depth-dependent quantities (*i.e.* the Lubberts

effect).[16] In order to include both direct and indirect detection, we use the term *secondary quanta* to refer to optical quanta or electron-hole pairs for the case of indirect and direct detection, respectively. Similarly to Bissonnette *et al.*,[12] we use the following stages: *1)* interaction of x-rays with the detector, which is a binary selection stage with probability equal to the x-ray quantum efficiency of the detector η_x; *2)* spread of ionizing radiation within the detector, a dislocation stage which has a Modulation Transfer Function (MTF) equal to $T_{rad}(f)$; *3)* creation of secondary quanta; an amplification stage with average gain $\overline{g}_{sec}$ and variance σ^2_{sec}; *4)* spread of secondary quanta, a dislocation stage which has an MTF equal to $T_{sec}(f)$; and *5)* loss of secondary quanta, a binary selection stage with probability η_{loss}. Following these stages, the analog DQE becomes

$$DQE_a(f) = \frac{\eta_x \eta_{loss}^2 \overline{g}_{sec}^2 |T_{rad}(f)|^2 |T_{sec}(f)|^2}{\eta_{loss}^2 \left[|T_{sec}(f)|^2 (\overline{g}_{sec}^2 + \sigma_{sec}^2) + (1 - |T_{sec}(f)|^2) \overline{g}_{sec} \right] + \eta_{loss}(1 - \eta_{loss}) \overline{g}_{sec}}$$

which simplifies to

$$DQE_a(f) = \eta_x \frac{\overline{g}_{sec}^2}{\overline{g}_{sec}^2 + \sigma_{sec}^2} |T_{rad}(f)|^2 \qquad (2)$$

in the limit $\overline{g}_{sec}$ >>1 which is the case for *a*-Se and Gd_2O_2S:Tb detectors where typically ~10^4 secondary quanta are created per interacting x-ray. The analog DQE of Eq. (2) represents the intrinsic DQE of a metal/phosphor or metal/photoconductor detector at megavoltage energies. In the approximation of the cascade analysis we have used, this DQE is thus seen to be degraded only by the x-ray quantum efficiency η_x, the variance σ^2_{sec} and the spread of ionizing radiation $T_{rad}(f)$, but not the spread of secondary quanta $T_{sec}(f)$ or the loss of secondary quanta η_{loss}.

In an AMFPI, the analog signal is first integrated over the active matrix pixels, and then sampled to create a digital signal. An electronic noise component S_e is then added to the noise power spectrum (NPS) by the flat panel, leading to a digital DQE for a direct or indirect AMFPI:

$$DQE_{dig}(f) = \frac{\eta_x |T_{rad}(f)|^2 |T_{sec}(f)|^2 \mathrm{sinc}^2(af)}{\left[\left(1 + \frac{\sigma_{sec}^2}{\overline{g}_{sec}^2} \right) |T_{sec}(f)|^2 \mathrm{sinc}^2(af) \otimes \sum_{j=-\infty}^{\infty} \delta\left(f - \frac{\eta_x}{d}\right) \cdot S_e \right]}$$

where

$$S_e = \frac{S_e}{\eta_x \eta_{loss}^2 \overline{g}_{sec}^2 a^4 q_0}$$

$\overline{g}_0$ is the incident fluence, *a* is the pixel size and *d* is the pixel pitch. For perfect flat-panel characteristics, *i.e.* infinitesimally small pixels and no electronic noise, the digital DQE reduces to the analog DQE. We refer to this as the *ideal* DQE for an AMFPI detector.

In order to calculate the DQE for both direct and indirect detectors at megavoltage energies, we need the quantities, *i.e.* η_x, $\overline{g}_{sec}$, σ^2_{sec}, and $T_{rad}(f)$. These quantities depend on the incident energy spectrum, and the densities, atomic numbers, and thicknesses of the front plate and sensitive layers. We determined these quantities for metal/phosphor and metal/*a*-Se detectors by Monte Carlo methods using EGSnrc.[17] The technical details have been previously described.[18] Briefly, two different types of simulations are used. The first type of simulation scores the energy absorbed in the sensitive region of the detector in order to determine the absorbed energy distribution (AED).[19] The quantum efficiency is then given by the zeroth-moment of the AED, and the quantities $\overline{g}_{sec}$ and σ^2_{sec} can be calculated using the first and second moments, respectively. The second set of simulations determine the spatial distribution of energy deposited in the sensitive region of the detector due to an infinitesimally thin line of incident x-rays. The resulting distribution corresponds to the LSF, from which we calculate $T_{rad}(f)$ using Fourier analysis.

In our calculations, we use an incident 6 MV spectrum as given by Kubsad *et al*.[20] The detectors for the indirect detection AMFPIs are modeled with a Cu front plate and a gadolinium oxysulfide Gd_2O_2S:Tb phosphor screen with a reduced density of 3.67 g/cm^3 as described by Jaffray *et al*.[19] For direct de-

tection, the front plate is modeled in the same fashion but the phosphor layer is replaced by atomic Se with a reduced density of 4.27 g/cm^3 to match that of the amorphous state. Describing *a*-Se in this fashion is an excellent approximation for studying macroscopic energy deposition only.[21]

For the case of direct detection, we use $T_{sec}(f)$=1. For indirect detection, we need the MTF describing the spread of visible light. For this purpose, we use the experimental MTFs for phosphor screens measured by Bissonnette *et al*.[13] These total MTFs $T_{tot}(f)$ are equivalent to the product

$$T_{tot}(f)=T_{rad}(f)T_{sec}(f). \quad (3)$$

To calculate $T_{sec}(f)$, we therefore divide the total experimental MTF by the MTF due to the spread of high energy radiation obtained by Monte Carlo techniques.

We first investigate what we have defined as the *ideal* DQE, *i.e.* the intrinsic DQE of metal/phosphor or metal/*a*-Se, given by Eq. (2). We calculate the ideal DQE as a function of spatial frequency for a 1 mm Cu front plate coupled with the following sensitive detectors: four phosphors of different mass thicknesses, namely 67 mg/cm^2 (Lanex Regular), 134 mg/cm^2 (Lanex Fast Back), 358 mg/cm^2, and 721 mg/cm^2; and four *a*-Se thicknesses, namely 46 mg/cm^2 (0.2 mm), 92 mg/cm^2 (0.4 mm), 138 mg/cm^2 (0.6 mm), and 184 mg/cm^2 (0.8 mm).

Once we have explored the ideal DQE, we use the results to explore the effects of the active matrix, *i.e.* pixel size, fill factor and electronic noise, using Eq. (3). In our calculations, for *a*-Se we assume that η_{loss} is governed only by recombination and assume a recombination fraction of 0.25.[22] For the case of phosphor we assume that η_{loss} is governed only by the absorption of visible light within the phosphor, and use the values tabulated by Bissonnette *et al*.[13] We assume that there are no further losses in the coupling of the secondary quanta to the active matrix array.

In order to validate our cascade analysis for AMFPI detectors, we calculate the DQE for the indirect AMFPI detector described by Munro and Bouius,[14] which consists of a 1.5 mm Cu front plate followed by a Lanex Fast Back phosphor screen (134 mg/cm^2 $Gd_2O_2S_4$:Tb). Their detector is placed on top a glass substrate which we include in our EGSnrc simulations. This glass substrate increases the energy deposited in the phosphor due to backscatter. Their active matrix is comprised of 0.75 mm pixels with a fill factor of 54%. They have determined that their detector is quantum limited at the exposures and spatial frequencies described in their paper, and we can thus neglect electronic noise in Eq. (3) for this case (for spatial frequencies below 1 cycle/mm).

To investigate the effects of aliasing and electronic noise, we calculate the DQE as a function of pixel size and electronic noise for two fill factors: 50% and 90%, for both direct and indirect detection techniques and with the same thicknesses described above for the case of the ideal DQE (the fill factor is defined as $F_p = a^2/d^2$).

Results

In Figure 1 we show the digital DQE we have calculated for the detector described by Munro and Bouius. We show excellent agreement to their data, which shows that the approximations we have used in the calculation of the DQE are justifiable.

In Figure 2 we show the ideal DQE(f) for indirect and direct detection methods respectively. The DQE(0) for each case can be seen to increase with mass thickness. The ideal DQE for both indirect and direct detection methods are degraded with spatial frequency only by the square of the MTF due to the spread of high energy radiation. This degradation is more pronounced as the mass thickness increases, but over the spatial frequency range shown, the ideal DQE(f) is superior for a larger mass thickness.

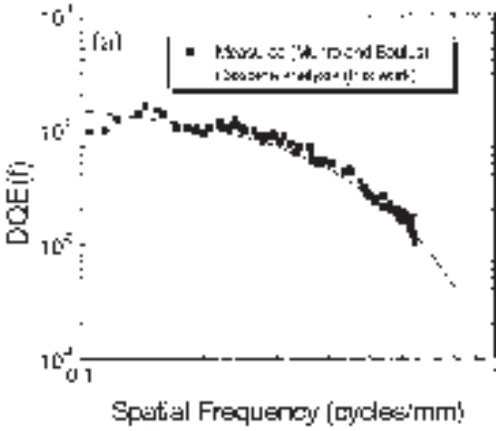

Figure 1. (a) DQE calculated from our cascade analysis for the indirect AMFPI described by Munro and Bouius, compared to their experimental data.

In order to show the effect of system noise and pixel size on the various detectors, we present our results as contour plots of the DQE normalized as a percentage of the ideal DQE. In this fashion, one can pick the appropriate design characteristics for a given detector, and visualize the corresponding degradation of the ideal DQE. The contour plots are shown at two reference spatial frequencies (0 and 1 cycles/mm) and for two fill factors (50% and 90%), for indirect detection and for direct detection AMFPIs in Figure 3 and Figure 4, respectively.

Discussion

For a given mass thickness, the ideal DQE is approximately the same for the direct and indirect methods, because as previously discussed, the NPS compensates for the degradation of the MTF. Since present practical phosphors generally have larger mass thicknesses than *a*-Se, the ideal DQEs shown are slightly greater for the indirect method. This can be overcome by increasing the thickness of *a*-Se to over 1 mm, which may however be technically difficult to attain while maintaining adequate uniformity of the *a*-Se.

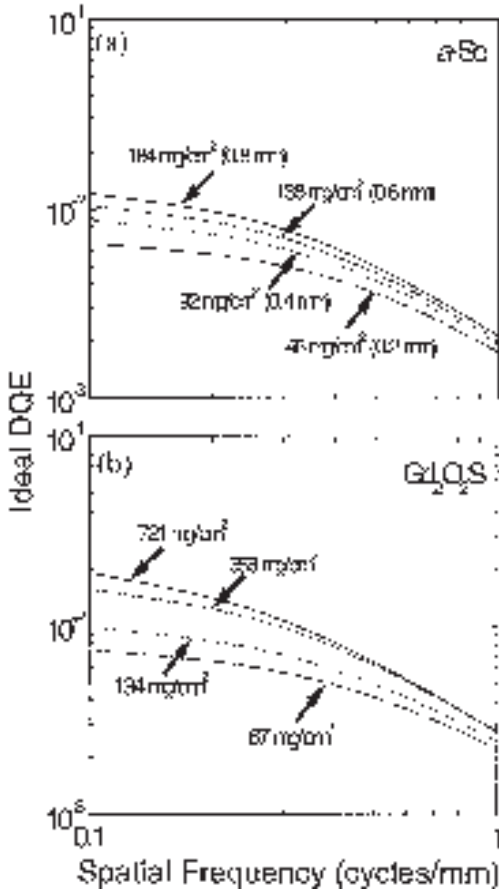

Figure 2. Ideal DQE (i.e. no system noise and no aliasing effects) for (a)direct (*a*-Se) and (b) indirect (Gd_2O_2S) AMFPIs. Theoretical calculations are for various phosphor thicknesses (a 1 mm Cu front plate and 6 MV photon beam are used).

By inspection of Figure 4, it can be seen that for indirect detection AMFPIs, the pixel size should be kept below about 0.3 mm and the electronic noise per incident fluence below about 10^5 mm^2 in order to ensure that the DQE is not significantly degraded. The fill factor is seen not to be an important factor for indirect detection detectors, as expected from the previous discussions.

For direct detection AMFPIs, the constraint on the pixel size is approximately the same as for indirect detection, but the electronic noise per incident fluence can be about

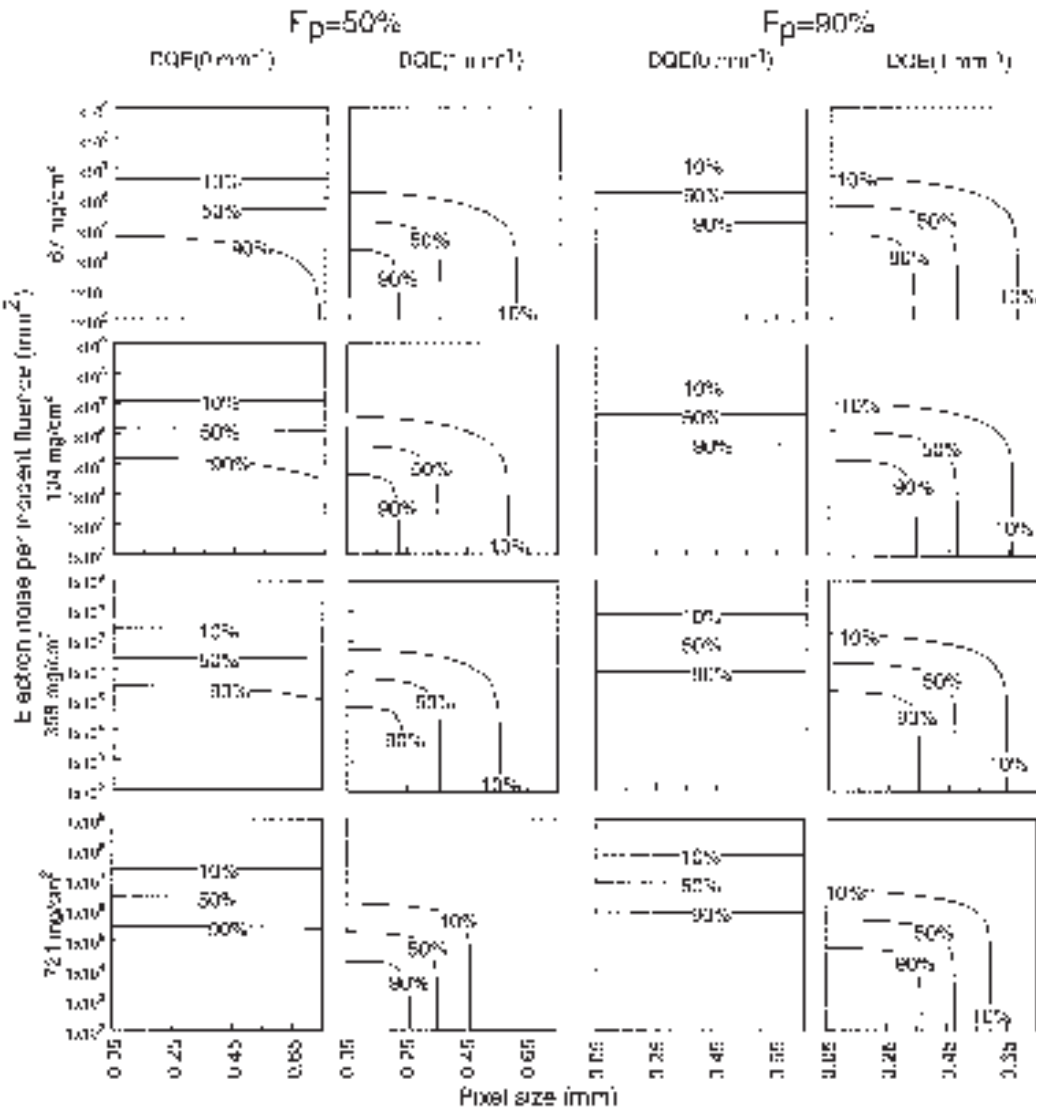

Figure 3. Contour plots of DQE at 0 and 1 cycles/mm, normalized as a percentage of the ideal DQE, for indirect AMFPIs as a function of pixel size and system noise per incident fluence. Plots are shown for both 50% and 90% fill factors, and for various phosphor thicknesses (a 1 mm Cu front plate and 6 MV photon beam are used).

two orders of magnitude greater than that for indirect detection, *i.e.* about 10^7 mm^2, before significantly degrading the DQE. It can also be seen, however, that the fill factor must be maximized for *a*-Se detectors. Several techniques have been discussed by Pang *et al.*[23] in order to increase the effective fill-factor.

The constraints on pixel size and electronic noise have been achieved in prototype detectors for diagnostic radiology, indicating that AMFPIs for portal imaging with DQEs equal to their ideal DQE can be manufactured. The AMFPI described by Munro *et al.* has been shown to be quantum limited, but

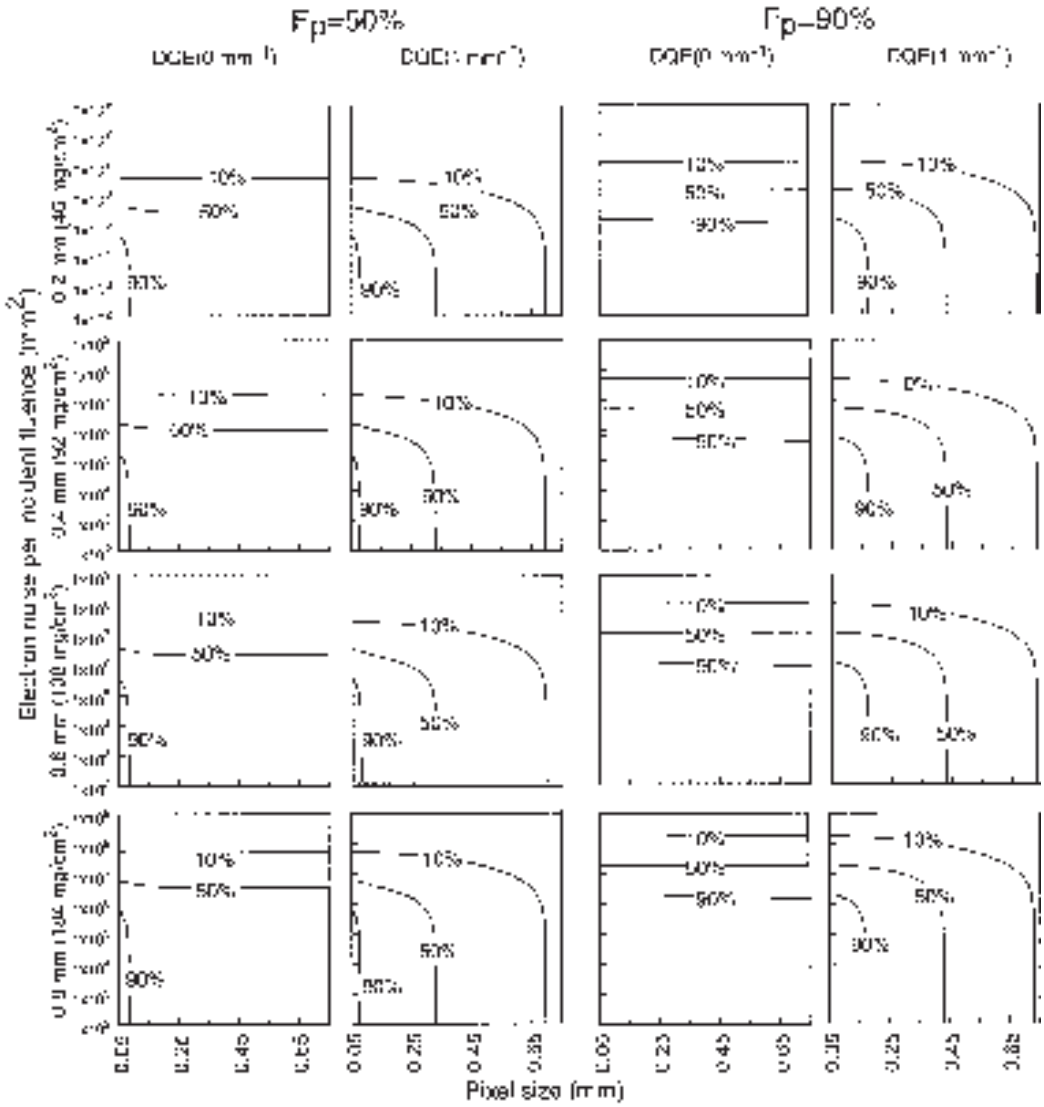

Figure 4. Contour plots of DQE at 0 and 1 cycles/mm, normalized as a percentage of the ideal DQE, for direct AMFPIs as a function of pixel size and system noise per incident fluence. Plots are shown for both 50% and 90% fill factors, and for various a-Se thicknesses (a 1 mm Cu front plate and 6 MV photon beam are used).

we have shown that its DQE could be improved if the pixel size were reduced from 0.75 mm to below 0.3 mm.

We have calculated the constraints on pixel size and electronic noise for both indirect and direct detection AMFPIs. In essence, if these constraints are satisfied, there is no significant advantage in using either the direct or indirect detection methods for megavoltage imaging. The main difference will likely be related to the manufacturing costs of building active matrices with specific pixel sizes, fill factors, and electronic noise. The cost and ease of manufacturing uniformly sensitive phosphors and *a*-Se layers must also be explored.

Conclusions

We have presented an approximation which describes the DQE of AMFPI detectors for portal imaging, for both direct and indirect detection methods. We validate our approximation with existing measurements of a prototype indirect-detection AMFPI and a metal/phosphor detector.

We calculate the ideal DQE for both direct and indirect detection AMFPIs for portal imaging. We show that although the resolution of the indirect detection method is superior to that of direct detection, the decrease in NPS compensates for this decrease in resolution.

We explore the effects of electronic noise, pixel size and fill factor for direct and indirect AMFPI detectors. We show that aliasing effects are more serious using the direct method, but that requirements on the electronic noise of the active matrix are more stringent for the indirect method. We show plots of the DQE as a function of system noise and pixel size for various detector thicknesses which should prove helpful in the design of future AMFPI detectors for portal imaging.

References

1. Kutcher GJ, Mageras GS, Leibel SA. Control, correction and modeling of setup errors and organ motion. *Semin Radiat Oncol* 1995; **5:** 143-5.

2. Essers M, Boellaard R, Van Herk M, Lanson H, Mijnheer B. Transmission dosimetry with a liquid-filled electronic portal imaging device. *Int J Radiat Oncol Biol Phys* 1996; **34:** 931-41.

3. Boellaard R, Herk Mv, Uiterwaal H, Mijnheer B. Two-dimensional exit dosimetry using a liquid-filled electronic portal imaging device and a convolution model. *Radiother Oncol* 1997; **44:** 149-157.

4. Boyer AL, Antonuk L, Fenster A, Van Herk M, Meertens H, Munro P, et al. A review of electronic portal imaging devices (EPIDs). *Med Phys* 1992; **19:** 1-16.

5. Munro P. Portal imaging technology: Past, present and future. *Semin Radiat Oncol* 1995; **5:** 115-33.

6. Antonuk LE, El-Mohri Y, Huang W, Jee K-W, Siewerdsen J, Maolinbay M, et al. Initial performance evaluation of an indirect-detection, active matrix flat-panel imager (AMFPI) prototype for megavoltage imaging. *Int J Rad Oncol Biol Phys* 1998; **42:** 437-52.

7. Zhao W, Blevis I, Germann S, Rowlands JA. Digital radiology using active matrix readout of amorphous selenium: Construction and evaluation of a prototype real-time detector. *Med Phys* 1997; **24:** 1834-43.

8. Kubo HD, Shapiro EG, Shapiro EJ. Potential and role of a prototype amorphous silicon array electronic portal imaging device in breathing synchronized radiotherapy. *Med Phys* 1999; **26:** 2410-4.

9. Cunningham IA. A spatial-frequency dependent quantum accounting diagram and detective quantum efficiency model of signal and noise propagation in cascaded imaging systems. *Med Phys* 1994; **21:** 417-27.

10. Siewerdsen JH, Antonuk LE, El-Mohri Y, Yorkston J, Huang W. Signal, noise power spectrum, and detective quantum efficiency of indirect-detection flat-panel imagers for diagnostic radiology. *Med Phys* 1998; **25:** 614-28.

11. Zhao W, Rowlands JA. Digital radiology using active matrix readout of amorphous selenium: Theoretical analysis of detective quantum efficiency. *Med Phys* 1997; **24:** 1819-33.

12. Bissonnette JP, Cunningham IA, Jaffray DA, Fenster A, Munro P. A quantum accounting and detective quantum efficiency analysis for video-based portal imaging. *Med Phys* 1997; **24:** 815-26.

13. Bissonnette J-P, Cunningham IA, Munro P. Optimal phosphor thickness for portal imaging. *Med Phys* 1997; **24:** 803-15.

14. Munro P, Bouius DC. X-ray quantum limited portal imaging using amorphous silicon flat-panel arrays. *Med Phys* 1998; **25:** 689-702.

15. Rabbani M, Shaw R. Detective quantum efficiency of imaging systems with amplifying and scattering mechanisms. *J Opt Soc Am* 1987; **4:** 895-901.

16. Lubberts G. Random noise produced by x-ray fluorescent screens. *J Opt Soc Am* 1968; **58:** 1475.

17. Nelson WR, Hirayama H, Rogers DWO. The EGS4 code system. *Stanford Linear Accelerator Center Report*, SLAC 265 1985.

18. Lachaine M, Fallone BG. Monte Carlo detective quantum efficiency and scatter studies of a metal/a-Se portal detector. *Med Phys* 1998; **25:** 1186-94.

19. Jaffray DA, Battista JJ, Fenster A, Munro P. Monte Carlo studies of x-ray energy absorption and quantum noise in megavoltage transmission radiography. *Med Phys* 1995; **22:** 1077-88.

20. Kubsad S, Mackie R, Gehring B, Misisco D, Paliwal B, Mehta M, et al. Monte Carlo and convolution dosimetry for stereotactic radiosurgery. *Int J Rad Onc Biol Phys* 1990; **19:** 1027-35.

21. Lachaine M, Fallone BG. Calculation of inelastic cross-sections for the interaction of electrons with amorphous selenium. *J Phys* D 2000; **33:** 551-5.

22. Mah D, Rowlands JA, Rawlinson JA. Sensitivity of amorphous selenium to x rays from 40 kVp to 18 MV: Measurements and implications for portal imaging. *Med Phys* 1998; **25:** 444-56.

23. Pang G, Zhao W, Rowlands JA. Digital radiology using active matrix readout of amorphous selenium: Geometric and effective fill factors. *Med Phys* 1998; **25:** 1636-46.